

A new series of short axially symmetrically and asymmetrically 1,3,6,8-tetrasubstituted pyrenes with two types of substituents: Syntheses, structures, photophysical properties and electroluminescence



Ran Zhang, Tengfei Zhang, Lu Xu, Fangfang Han, Yun Zhao, Zhonghai Ni*

School of Chemical Engineering and Technology, China University of Mining and Technology, Xuzhou 221116, People's Republic of China

ARTICLE INFO

Article history:

Received 22 February 2016

Received in revised form

9 July 2016

Accepted 25 July 2016

Available online 28 July 2016

Keywords:

Pyrene-based compounds

Molecular configurations

Photoluminescence

Electroluminescence

ABSTRACT

A new series of short axially symmetrically (**4a** and **4b**) and asymmetrically (**4c** and **4d**) 1,3,6,8-tetrasubstituted pyrene-based compounds with two phenyl moieties and two diphenylamine units on the pyrene core were designed and synthesized based on stepwise synthetic strategy. These compounds were structurally characterized and their photoelectric properties were investigated by spectroscopy, electrochemical and theoretical studies. The structures of **4a** and **4b** were determined by single-crystal X-ray diffraction analysis, indicating that the compounds are twisted by the peripheral substituents and the intermolecular π - π interactions have been efficiently interrupted. The four compounds exhibit high absolute fluorescence quantum yields (Φ_F) in dichloromethane (83.31–88.45%) and moderate Φ_{FS} in film states (20.78–38.68%). In addition, compounds **4a** and **4b** display relatively higher absolute Φ_{FS} than those of **4c** and **4d** in film states. All the compounds exhibit high thermal stability with decomposition temperatures above 358 °C and the values of **4c** and **4d** are higher than **4a** and **4b**. Compounds **4a** and **4b** can form morphologically stable amorphous thin films with T_g values of 146 °C and 149 °C, respectively. However, there are no obvious T_g observed in compounds **4c** and **4d**. Electroluminescent devices using **4a** and **4b** as doped emission layer show promising device performance with low turn-on voltage (3.0 V), maximum brightness around 15100 cd/m² and 16100 cd/m², maximum luminance efficiency of 12.4 cd/A and 13.6 cd/A and maximum external quantum efficiency of 5.34% and 5.63%, respectively.

© 2016 Elsevier B.V. All rights reserved.

1. Introduction

Pyrene as one of the most known polyaromatic hydrocarbons (PAHs) has been paid everlasting attention in the development of organic fluorescent materials [1–5]. In recent years, numerous investigations have been carried out on the design and synthesis of pyrene-based compounds and their applications in organic light-emitting diodes (OLEDs), organic field-effect transistors (OFETs), and organic photovoltaic devices (OPVs) because of their excellent fluorescence property, outstanding thermal stability, high charge carrier mobility and hole-injection ability [6–11]. To develop more excellent pyrene-based materials, the effective strategy is to tune the molecular structures and the photoelectric properties by

introducing different peripheral attachments into the suitable positions of pyrene core [10,12,13]. Indeed, a larger number of pyrene-based compounds with various peripheral groups and interesting photoelectric properties have been synthesized and exploited as efficient emitting and transporting materials for high performance photoelectric devices [10,14–17]. Furthermore, some pyrene-based materials have been exploited as emitters for conventional solution-processed organic electronic devices, since they have sufficient solubility and good film-forming abilities [18–20].

Among the many different modification methods on the pyrene core for novel pyrene-based photoelectric materials, the 1,3,6,8-tetrasubstituted pyrene-base compounds have the special advantages which facilitates not only the controlling on the intermolecular interactions but also the intramolecular electronic distribution [3,21–23]. For example, the incorporation of phenyl moieties, ethynyl groups and trimethylsilyl units at the 1,3,6,8-positions in pyrene can twist the structure and prevent excimer formation,

* Corresponding author.

E-mail address: nizhonghai@cumt.edu.cn (Z. Ni).

resulting in dramatic improvement in the photoluminescence properties, especially in the fluorescence quantum yield [24–28]. However, to the best of our knowledge, most of the reported 1,3,6,8-tetrasubstituted pyrene compounds are modified using the same substituents. There are very few examples of symmetrically and asymmetrical 1,3,6,8-tetrasubstituted pyrenes with different peripheral segments on the pyrene ring due to the difficulty in synthesis and separation [16,23].

Based on the above considerations, we designed and synthesized a series of short axially symmetrically and asymmetrically 1,3,6,8-tetrasubstituted pyrenes with two phenyl moieties and two diphenylamine units on the pyrene core through the stepwise derivatization and functional transformation strategy using pyrene as the precursor (Scheme 1). The intermolecular interactions between the planar pyrene rings can be prevented by the peripheral phenyl segments and diphenylamine groups and the incorporation of arylamine units can improve the hole-injection and hole-transporting capability of the materials. Moreover, such architectures with two different substituents can more efficiently optimize the intramolecular electron distribution than those of 1,3,6,8-tetrasubstituted pyrenes with the same peripheral groups [16,29,30]. Herein, we report the design, synthesis, photoelectrical and electroluminescence properties of short axially symmetrically and asymmetrically 1,3,6,8-tetrasubstituted pyrenes with two types of substituents.

2. Experimental section

2.1. General

Dichloromethane was distilled from calcium hydride. All other chemicals were purchased from commercial sources and used without further purification. ^1H and ^{13}C NMR spectra were collected on a Bruker-400 MHz or Bruker-600 MHz spectrometer in CDCl_3 solution with TMS as an internal standard. Mass spectra were obtained on a Bruker Ultraflex extreme MALDI TOF/TOF mass spectrometer. Elemental analysis (C, H, N) of the dried solid samples were carried out using an Elementary Vario El analyzer. UV–Vis spectra were recorded on Shimadzu UV-3600 with a UV-VIS-NIR spectrophotometer. Emission spectra were performed by a HITACHI fluorescence spectrometer (F-4600). The absolute fluorescence quantum yields (Φ_F) were determined by FM-4P-TCSPC Transient State Fluorescence Spectrometer using an integrating sphere for dilute dichloromethane and thin films which obtained by drop-casting on quartz plate. Cyclic voltammetry experiments were performed with a CHI660A electrochemical work station. All measurements were carried out at room temperature with a conventional three-electrode configuration consisting of a glassy

carbon working electrode, a platinum auxiliary electrode and a calomel reference electrode. The solvent in all experiments was dry dichloromethane and the supporting electrolyte was 0.1 M tetrabutylammonium hexafluorophosphate. The glass-transition temperatures (T_g) of the compounds were determined with differential scanning calorimetry (DSC) under a nitrogen atmosphere by using a DSC6000 (PerkinElmer). Samples were heated to 400 °C at a rate of 10 °C min^{-1} and cooled at 10 °C min^{-1} then heated again under the same heating conditions as used in the initial heating process, the values of T_g were determined from the second heating scan. Decomposition temperatures (T_d) were determined with thermogravimetric analysis (TGA) under a nitrogen atmosphere by using a DTG-60AH (Shimadzu). Samples were heated to 700 °C at a rate of 10 °C min^{-1} . Crystals data of compounds were selected on a Bruker APEX II CCD diffractometer with graphite-monochromated Mo-K α radiation ($\lambda = 0.71073 \text{ \AA}$) at 293 K using the ω -scan technique. The structures were solved by direct methods with the SHELXS-97 computer program, and refined by full-matrix least-squares methods (SHELXL-97) on F^2 [31]. The ground state geometries of all molecules were fully optimized using density functional theory (DFT) at the B3LYP/6-31G (d,p) level, as implemented in Gaussian 09 W software package [32]. The electronic transitions were calculated using the time-dependent DFT (B3LYP) theory and the 6-31G (d, p) basis set.

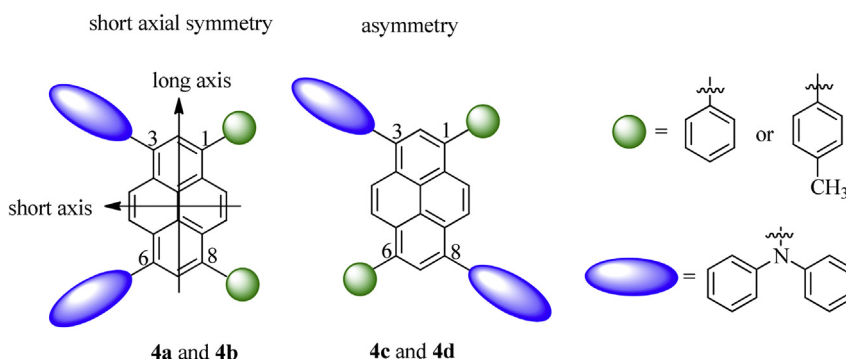
2.2. OLED fabrication and performance evaluation

ITO-coated glasses with a sheet resistance of 30 Ω per square were used as substrates. Before the devices were fabricated, the substrates were first cleaned with acetone, ethanol, and deionized water. Then, they were oven-dried at 120 °C and treated with UV-ozone under ambient conditions for 5 min. Finally, the cleaned glasses were transferred to a vacuum deposition system at approximately 4×10^{-4} Torr. Thermally evaporated organic layers were sequentially grown onto the ITO substrates at a rate of $1\text{--}2 \text{ \AA s}^{-1}$. The cathode was completed via the thermal deposition of Cs_2CO_3 at a rate of 0.1 \AA s^{-1} and then covered with Al metal deposited at a rate of 10 \AA s^{-1} . EL luminances and spectra were obtained using an AvaSpec-ULS2048L fiber spectrometer, and the current–voltage characteristics were determined with a computer-controlled Keithley 4200 SCS in ambient atmosphere. EQE was calculated from the current density, luminance, and EL spectrum, assuming a Lambertian distribution.

2.3. Synthesis

2.3.1. Synthesis of 1,8-diphenylpyrene (2a)

Under the atmosphere of nitrogen, the mixture of 1,8-



Scheme 1. The strategy for new 1,3,6,8-tetrasubstituted pyrene-based photoelectric materials (4a–4d).

dibromopyrene (85%) and 1,6-dibromopyrene (15%) (1.80 g, 5 mmol) [33], phenylboronic acid (1.46 g, 12 mmol), Pd(PPh₃)₄ (0.12 g, 0.1 mmol) and 2 M potassium carbonate solution (12 mL) were dissolved in toluene (80 mL) and refluxed for 24 h. After the reaction was finished, the mixture was poured into water and extracted with dichloromethane. The organic layer was dried over MgSO₄ and the solvent was removed under vacuum. Then, the crude products were purified by silica gel column chromatography using hexane/dichloromethane mixture as eluent afforded a mixture of **2a** and **2c**. Finally, the mixture was recrystallized from dichloromethane/ethanol (2:3) solution and the pure compound **2a** was obtained as white solid. Yield: 1.15 g, 65%. ¹H NMR (600 MHz, CDCl₃) δ 8.23 (d, *J* = 7.8 Hz, 2H), 8.12 (d, *J* = 11.1 Hz, 4H), 7.99 (d, *J* = 7.8 Hz, 2H), 7.63–7.60 (m, 4H), 7.53 (t, *J* = 7.6 Hz, 4H), 7.45 (t, *J* = 7.4 Hz, 2H). ¹³C NMR (151 MHz, CDCl₃) δ 141.15 (s), 137.62 (s), 130.94 (s), 130.62 (s), 128.37 (s), 127.85–126.96 (m), 125.41 (s), 125.25 (s), 124.83 (s). MALDI TOF-MS: *m/z* 354.171 [M]⁺. Elemental analysis: anal. Calcd for C₂₈H₁₈: C, 94.88; H, 5.12; Found: C, 94.93; H, 5.08.

2.3.2. Synthesis of 1,8-bis(4-methylphenyl)pyrene (**2b**)

The compound was synthesized with the same method as for compound **2a** by using 4-methylphenylboronic acid (1.63 g, 12 mmol). Accordingly, the pure compound **2b** was obtained by recrystallizing from dichloromethane/ethanol (1:2) mixture as white solid. Yield: 1.21 g, 65%. ¹H NMR (400 MHz, CDCl₃) δ 8.25 (d, *J* = 8.0 Hz, 2H), 8.15 (d, *J* = 16.8 Hz, 4H), 8.01 (d, *J* = 8.0 Hz, 2H), 7.55 (d, *J* = 8.0 Hz, 4H), 7.38 (d, *J* = 8.0 Hz, 4H), 2.51 (s, 6H). ¹³C NMR (101 MHz, CDCl₃) δ 150.10 (s), 138.13 (s), 137.50 (s), 130.79 (s), 130.27 (s), 128.44 (s), 127.66 (s), 127.34 (s), 125.63–124.99 (m), 124.71 (s), 34.66 (s), 31.48 (s). MALDI TOF-MS: *m/z* 382.215 [M]⁺. Elemental analysis: anal. calcd for C₃₀H₂₂: C, 94.20; H, 5.80; Found: C, 94.31; H, 5.72.

2.3.3. Synthesis of 1,6-diphenylpyrene (**2c**)

A mixture of 1,6-dibromopyrene (1.80 g, 5 mmol), phenylboronic acid (1.46 g, 12 mmol), Pd(PPh₃)₄ (0.12 g, 0.1 mmol) and 2 M potassium carbonate solution (12 mL) in toluene (80 mL) was heated to reflux for 24 h under nitrogen. After the reaction was finished, the mixture was poured into water and extracted with dichloromethane. The organic layer was dried over MgSO₄ and the solvent was removed under vacuum. Then, the crude products were purified by silica gel column chromatography using hexane/dichloromethane mixture as eluent afforded **2c** as white plate crystals. Yield: 1.6 g, 90%. ¹H NMR (400 MHz, CDCl₃) δ 8.23 (dd, *J* = 8.5, 5.8 Hz, 4H), 8.05 (dd, *J* = 20.9, 8.5 Hz, 4H), 7.71–7.65 (m, 4H), 7.60 (t, *J* = 7.4 Hz, 4H), 7.52 (t, *J* = 7.3 Hz, 2H). ¹³C NMR (101 MHz, CDCl₃) δ 141.29 (s), 137.85 (s), 130.62 (s), 130.41 (s), 128.84 (s), 128.38 (s), 127.78 (s), 127.47 (s), 127.25 (s), 125.30 (s), 125.20 (s), 124.49 (s), 29.72 (s). MALDI TOF-MS: *m/z* 354.154 [M]⁺. Elemental analysis: anal. calcd for C₂₈H₁₈: C, 94.88; H, 5.12; Found: C, 94.94; H, 5.07.

2.3.4. Synthesis of 1,6-bis(4-methylphenyl)pyrene (**2d**)

The compound was synthesized with the same method as for compound **2c** by using 4-methylphenylboronic acid (1.63 g, 12 mmol). Accordingly, the pure compound **2d** was obtained as white powder solid. Yield: 1.62 g, 92%. ¹H NMR (400 MHz, CDCl₃) δ 8.22 (dd, *J* = 8.4, 6.3 Hz, 4H), 8.03 (dd, *J* = 21.3, 8.5 Hz, 4H), 7.57 (d, *J* = 7.9 Hz, 4H), 7.41 (d, *J* = 7.8 Hz, 4H), 2.54 (s, 6H). ¹³C NMR (101 MHz, CDCl₃) δ 138.37 (s), 137.79 (s), 136.95 (s), 130.50 (s), 130.30 (s), 129.10 (s), 128.89 (s), 127.77 (s), 127.35 (s), 125.29 (s), 125.25 (s), 124.41 (s), 29.72 (s), 21.31 (s). MALDI TOF-MS: *m/z* 382.212 [M]⁺. Elemental analysis: anal. calcd for C₃₀H₂₂: C, 94.20; H, 5.80; Found: C, 94.28; H, 5.74.

2.4. General procedure for the synthesis of compounds **3a–3d**

Br₂ (6.3 mmol) in 15 mL DMF was added dropwise into the solution of **2** (3 mmol) in 15 mL DMF. After stirring for 10 h at room temperature, water was added. The precipitated solid was collected and then recrystallized from toluene and ethanol solutions.

3,6-dibromo-1,8-diphenylpyrene (**3a**) was obtained as a faint yellow solid after recrystallization from toluene and ethanol (3:1) mixture. Yield: 1.47 g, 96%. MALDI TOF-MS: *m/z* 512.2 [M]⁺.

3,6-dibromo-1,8-bis-(4-methylphenyl)pyrene (**3b**) was obtained as a faint yellow solid after recrystallization from toluene and ethanol (2:1) mixture. Yield: 1.59 g, 98%. MALDI TOF-MS: *m/z* 540.0 [M]⁺.

3,8-dibromo-1,6-diphenylpyrene (**3c**) was obtained as a faint yellow solid after recrystallization from toluene. Yield: 1.49 g, 97%. MALDI TOF-MS: *m/z* 512.3 [M]⁺.

3,8-dibromo-1,6-bis-(4-methylphenyl)pyrene (**3d**) was obtained as a faint yellow solid after recrystallization from toluene. Yield: 1.59 g, 98%. MALDI TOF-MS: *m/z* 539.9 [M]⁺.

2.5. General procedure for the synthesis of the compounds **4a–4d**

Under the atmosphere of nitrogen, a mixture of **3** (2.5 mmol), diphenylamine (1.02 g, 6 mmol), bis(dibenzylideneacetone)palladium (Pd(dba)₂) (48 mg, 0.05 mmol), P(*t*-Bu)₃ (0.1 g/mL in toluene, 0.15 mL, 0.075 mmol), sodium tert-butoxide (0.58 g, 6 mmol) and toluene (50 mL) were heated at 80 °C for 4–5 h. After it cooled, water and dichloromethane were added and the organic layer was separated. Then, the organic layer was dried over MgSO₄ and the solvent was removed under vacuum. The crude products were purified by silica gel column chromatography using hexane/dichloromethane mixture as eluent.

3,6-bis(*N,N*-diphenyl)-1,8-diphenylpyrene (**4a**) was obtained as a yellow powder solid (silica gel column chromatography from hexane: dichloromethane = 60:1). Yield: 1.46 g, 85%. ¹H NMR (400 MHz, CDCl₃) δ 8.13 (d, *J* = 5.5 Hz, 4H), 7.85 (s, 2H), 7.60–7.50 (m, 10H), 7.23–7.21 (m, 8H), 7.19–7.09 (m, 8H), 6.95 (t, *J* = 7.3 Hz, 4H). ¹³C NMR (101 MHz, CDCl₃) δ 148.50 (s), 140.50 (d, *J* = 10.9 Hz), 138.99 (s), 130.53 (s), 129.70 (s), 129.17 (s), 128.36 (s), 128.08 (s), 127.49–126.91 (m), 124.95 (s), 123.76 (s), 122.07 (s), 121.79 (s). MALDI TOF-MS: *m/z* 688.3 [M]⁺. Elemental analysis: anal. calcd for C₅₂H₃₆N₂: C, 90.67; H, 5.27; N, 4.07; Found: C, 90.58; H, 5.31; N, 4.09.

3,6-bis(*N,N*-diphenyl)-1,8-bis-(4-methylphenyl)pyrene (**4b**) was obtained as a yellow powder solid (silica gel column chromatography from hexane: dichloromethane = 20:1). Yield: 1.56 g, 87%. ¹H NMR (400 MHz, CDCl₃) δ 8.12 (d, *J* = 18.8 Hz, 4H), 7.83 (s, 2H), 7.49 (d, *J* = 8.0 Hz, 4H), 7.33 (d, *J* = 7.6 Hz, 4H), 7.22–7.18 (m, 8H), 7.13–7.08 (m, 8H), 6.95 (t, *J* = 7.4 Hz, 4H), 2.48 (s, 6H). ¹³C NMR (101 MHz, CDCl₃) δ 148.52 (s), 140.47 (s), 138.92 (s), 137.56 (s), 137.19 (s), 130.41 (s), 129.73 (s), 129.11 (d, *J* = 7.4 Hz), 127.95 (s), 127.31 (s), 127.15 (s), 124.93 (s), 123.66 (s), 122.05 (s), 121.74 (s), 21.27 (s). MALDI TOF-MS: *m/z* 716.3 [M]⁺. Elemental analysis: anal. calcd for C₅₄H₄₀N₂: C, 90.47; H, 5.62; N, 3.91; Found: C, 90.35; H, 5.73; N, 3.81.

3,8-bis(*N,N*-diphenyl)-1,6-diphenylpyrene (**4c**) was obtained as a yellow powder solid (silica gel column chromatography from hexane: dichloromethane = 15:1). Yield: 1.34 g, 78%. ¹H NMR (400 MHz, CDCl₃) δ 8.15 (d, *J* = 9.6 Hz, 2H), 8.07 (d, *J* = 9.2 Hz, 2H), 7.85 (s, 2H), 7.57–7.43 (m, 10H), 7.22 (t, *J* = 8.4 Hz, 8H), 7.11 (d, *J* = 8.0 Hz, 8H), 6.96 (t, *J* = 7.6 Hz, 4H). ¹³C NMR (101 MHz, CDCl₃) δ 148.55 (s), 140.41 (s), 139.16 (s), 130.52 (s), 129.60 (s), 129.21 (s), 128.33 (s), 127.76 (s), 127.41–127.31 (m), 125.63 (s), 123.08 (s), 122.06 (s), 121.79 (s). MALDI TOF-MS: *m/z* 688.3 [M]⁺. Elemental analysis: anal. calcd for C₅₂H₃₆N₂: C, 90.67; H, 5.27; N, 4.07; Found:

C, 90.72; H, 5.24; N, 4.04.

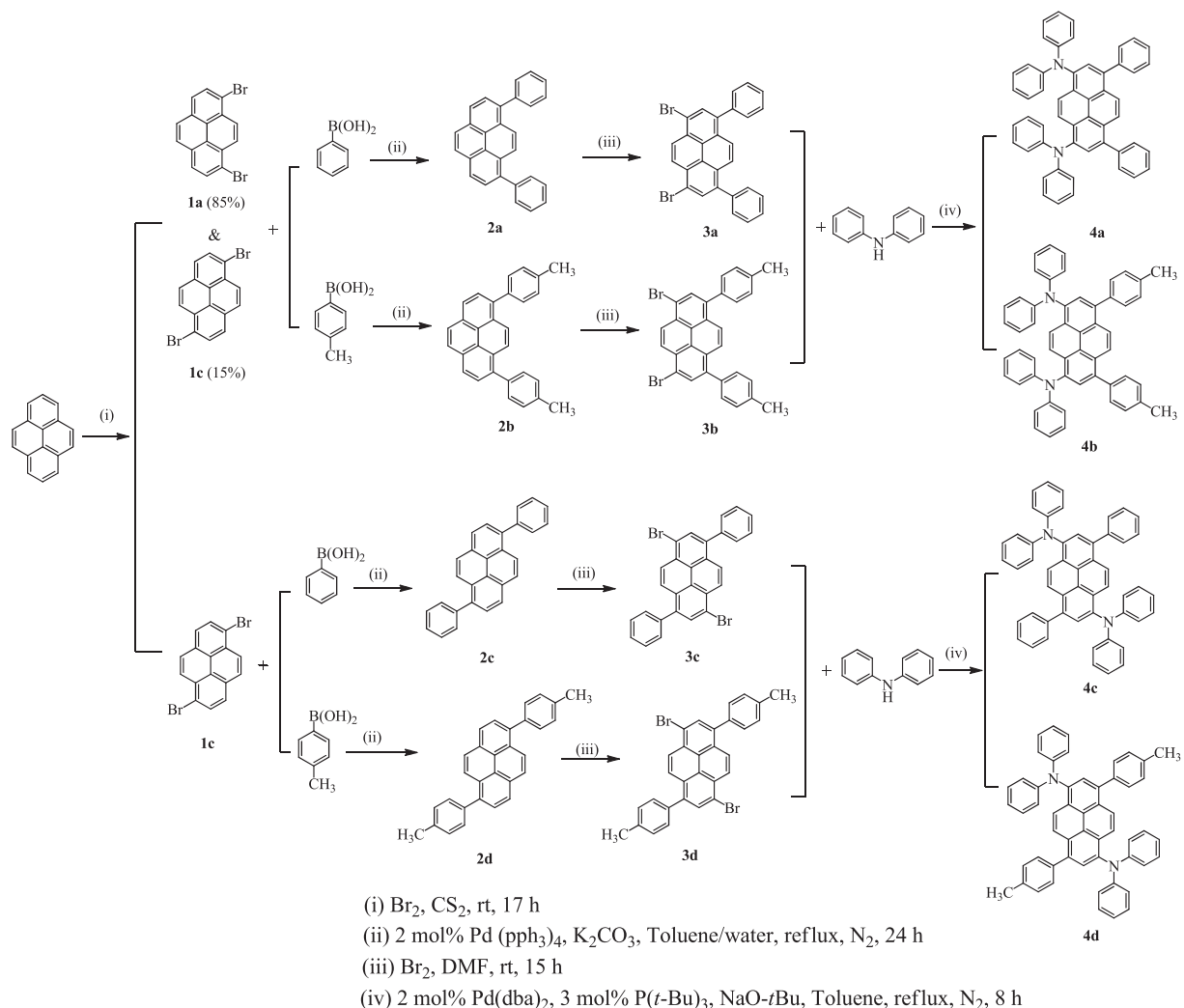
3,8-bis(*N,N*-diphenyl)-1,6-bis(4-methylphenyl)pyrene (**4d**) was obtained as a yellow powder solid (silica gel column chromatography from hexane: dichloromethane = 20:1). Yield: 1.34 g, 75%. ¹H NMR (400 MHz, CDCl₃) δ 8.09 (dd, *J* = 8.0 Hz, 9.6 Hz, 4H), 7.81 (s, 2H), 7.44 (d, *J* = 8.0 Hz, 4H), 7.30 (s, 4H), 7.23–7.18 (m, 8H), 7.10 (d, *J* = 7.6 Hz, 8H), 6.94 (t, *J* = 7.8 Hz, 4H), 2.44 (s, 6H). ¹³C NMR (101 MHz, CDCl₃) δ 148.51 (s), 140.47 (s), 138.92 (s), 137.37 (d, *J* = 36.4 Hz), 130.41 (s), 129.73 (s), 129.11 (d, *J* = 7.3 Hz), 127.95 (s), 127.23 (d, *J* = 15.9 Hz), 124.93 (s), 123.66 (s), 122.05 (s), 121.74 (s), 21.27 (s). MALDI TOF-MS: *m/z* 716.4 [M]⁺. Elemental analysis: anal. calcd for C₅₄H₄₀N₂: C, 90.47; H, 5.62; N, 3.91; Found: C, 90.27; H, 5.57; N, 3.89.

3. Results and discussion

3.1. Synthesis

The synthetic routes of the intermediates and target compounds are shown in Scheme 2 using pyrene as the starting material. Firstly, bromination of pyrene afforded a mixture of 1,8-dibromopyrene (**1a**) and 1,6-dibromopyrene (**1c**) as reported in the literature [33]. The mixture isolated by fractional recrystallization from toluene into two components and the less soluble pure 1,6-

dibromopyrene was obtained, but regrettably, the relatively more soluble 1,8-dibromopyrene fraction still contained a small amount of 1,6-dibromopyrene (15%). The continuous separation of 1,6- and 1,8-dibromopyrenes are tedious and difficult due to the slight difference in solubility of the dibromopyrenes. Therefore, we start the experiments using the impure 1,8-dibromopyrene because it is possible to obtain the final pure 1,8-disubstituted pyrene-based compounds in the flowing steps. Secondly, the pure 1,6-dibromopyrene was changed to **2c** and **2d** easily by Suzuki coupling reaction with high yields. Accordingly to the same method, the mixture of 85% 1,8-dibromopyrene and 15% 1,6-dibromopyrene were transformed to the key intermediates **2a** and **2b** respectively containing slight **2c** and **2d**. There are significant differences of solubility between **2a** and **2c**, **2b** and **2d**, and therefore the pure key intermediates **2a** and **2b** were relatively readily obtained from recrystallization. Thirdly, compounds **2a–2d** were brominated with liquid bromine, yielding another key intermediates **3a–3d** in very high yields above 95%. The presence of two bromide substituents drastically reduced the solubility of the compounds, which fails to obtain the detailed characterizations of **3a–3d**. Finally, the target products **4a–4d** were prepared by Buchwald–Hartwig coupling reaction between the compound **3** and diphenylamine with yields of 80–90%. Compounds **4a** and **4b** show excellent solubility in common organic solvents, but the



Scheme 2. Procedures for the syntheses of compounds **4a–4d**.

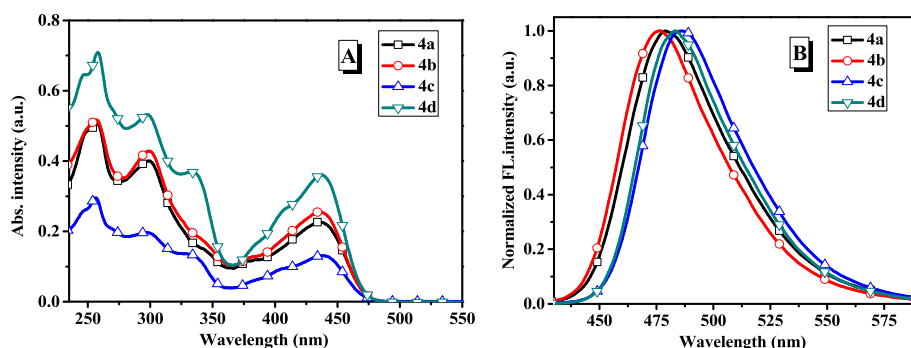


Fig. 1. Absorption (A) and normalized emission spectra (B, excitation wavelength: 410 nm) of the compounds **4a–4d** recorded in dichloromethane at 1×10^{-5} M concentration.

solubilities of **4c** and **4d** are very poor, which indicates that the symmetrical configuration of pyrene can significantly increase the solubility. The solubilities of compounds **4a–4d** in various solvents (mg/ml) are listed in Table S1. The poor solubility limits the synthesis and purification of more new asymmetrically 1,3,6,8-tetrasubstituted pyrene-based photoelectric materials. Furthermore, the X-ray diffraction patterns (Fig. S1) for drop-casting film samples of compounds **4a** and **4b** show representative broad diffuse band, indicating that **4a** and **4b** can form amorphous thin films. However, the diffraction patterns for film samples of **4c** and **4d** exhibit sharp peaks, demonstrating that the films of **4c** and **4d** are crystalline state.

3.2. Photophysical properties

The UV–vis absorption and photoluminescence (PL) spectra of compounds **4a–4d** in dilute dichloromethane are shown in Fig. 1. The detailed photophysical data are presented in Table 1. The absorptions of compounds **4a** and **4b** have some differences with **4c** and **4d**. Compounds **4c** and **4d** exhibit small red-shift compared with those of **4a** and **4b** and the absorption fine structures of **4c** and **4d** are more obvious than those of **4a** and **4b**, which indicates that the different molecular configurations have some effects on the absorptions of the compounds. The compounds **4a–4d** feature the longest wavelength absorptions at ca. 436–439 nm maybe attributed to the charge transfer from pyrenylamine to pyrene. The absorptions for compounds **4a–4d** at ca. 332–334 nm probably ascribed to the charge transfer from diphenylamine units to pyrene. However, the absorptions of **4a** and **4b** are very weaker than those of **4c** and **4d**. It is probably caused by the different charge distribution which is attribute to the different molecule configuration. The higher energy bands appearing at ca. 297–299 nm may be assigned to pyrene and phenyl localized $\pi-\pi^*$ transitions [34]. The intense bands of **4a–4d** appearing at ca. 256 nm probably stem from phenyl ring present in the molecule [35].

The PL spectra of compounds **4a–4d** in dichloromethane display emission peak in green region. The symmetrical compounds **4a** and

4b display blue-shift relative to those of asymmetrical compounds **4c** and **4d**, indicating that the symmetrical configuration can reduce the π -conjugation of the compounds to some extent. Compound **4b** exhibits slightly red-shift compared with that of **4a**, which demonstrates that the incorporation of methyl groups increases the π -conjugation of the molecules, similarly, compound **4d** also shows minor red-shift than that of **4c**. Compounds **4a–4d** show small Stokes shifts ($1927\text{--}2203\text{ cm}^{-1}$ in dichloromethane), indicating less energy loss during the relaxation process and thereby ensuring efficient fluorescence. As shown in Fig. 2, the emission spectra of these compounds in thin films exhibit obvious bathochromic shift relative to those in dichloromethane solution with the values of 55 nm, 24 nm, 32 nm and 19 nm for **4a**, **4b**, **4c** and **4d**, respectively, suggesting that there exists intermolecular $\pi-\pi$ interactions in film state. Compounds **4b** and **4d** are blue-shift than those **4a** and **4c**, respectively, stating that the introduction of methyl groups can increase the molecular twist and weaken the intermolecular $\pi-\pi$ interactions. The red-shifts of **4a** and **4b** are larger than **4c** and **4d**, respectively, which may indicate that the asymmetrical structure is more beneficial to interrupt the intermolecular $\pi-\pi$ interactions. The PL spectra of the four compounds have no obvious trailing at long wavelengths, indicating that the formation of an excimer or exciplex can be effectively suppressed, other than some pyrene-based materials [36–39]. It is probably because that the peripheral substituents twist the molecular backbone and suppress the intermolecular interactions [16,17,29,30]. The absolute fluorescence quantum yields Φ_{FS} of compounds **4a–4d** in dichloromethane and in film state were determined using an integrating sphere. These compounds show high Φ_{FS} in dichloromethane with the range from 83.31 to 88.45%. The Φ_{FS} of compounds **4a–4d** in film states (20.78–38.68%) show a decreasing tendency compared to those in dichloromethane due to the intermolecular interactions in film states. Compounds **4b** and **4d** exhibit higher Φ_{FS} than those of **4a** and **4c**, indicating that the introduction of methyl groups to peripheral phenyl ring can more effectively prevent the intermolecular interactions. Moreover, the Φ_{FS} of **4a** and **4b** are higher than **4c** and **4d**, demonstrating that the

Table 1
Physical parameters of the compounds **4a–4d**.

Com.	$\lambda_{\text{abs}}^{\text{a}}$ (nm)	$\lambda_{\text{em}}^{\text{a}}$ (nm)/($\Phi_{\text{F}}^{\text{c}}$ (%))	$\lambda_{\text{em}}^{\text{b}}$ (nm)/($\Phi_{\text{F}}^{\text{c}}$ (%))	Stokes shift (cm^{-1})
4a	257, 299, 340, 436	479 (88.45)	534 (31.57)	2059
4b	257, 299, 340, 436	476 (85.31)	500 (38.68)	1927
4c	256, 297, 333, 439	486 (83.31)	518 (20.78)	2203
4d	258, 298, 332, 437	483 (84.35)	502 (27.45)	2179

^a Measured in dichloromethane.

^b Measured as drop-coated film.

^c Absolute quantum yield measured using integrating sphere.

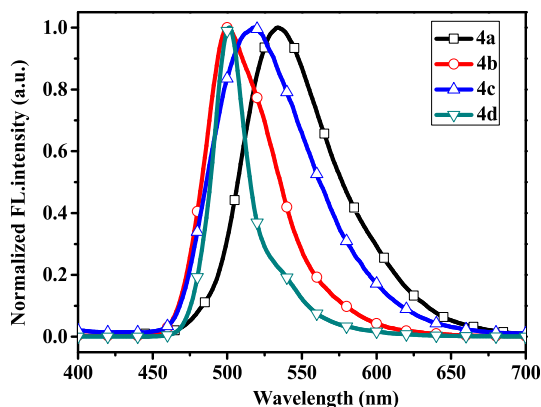


Fig. 2. Normalized emission spectra of the compounds **4a–4d** recorded as thin films (excitation wavelength: 390 nm).

symmetrical structure is more beneficial to improve the PL properties.

To better understand the effect of environments on the electronic spectroscopies of the compounds, we study the absorption and emission spectra of compounds **4a–4d** in different polar solvents such as toluene (TOL), dichloromethane (DCM), tetrahydrofuran (THF), methanol (MeOH), *N,N*-dimethylformamide (DMF) and acetonitrile (MeCN). The pertinent data are summarized in Table S2 and Table S3. The changes in absorption and emission

profiles for compound **4a–4d** with different solvent polarities are illustrated in Figs. S2–S5. The absorption spectra show the four compounds are insensitive to the solvent polarity with the shift below 8 nm. In the emission spectra, compounds **4a–4d** display a remarkable and positive solvatochromism, which indicates that the excited state is more stable in polar solvent probably due to the separation of charges in the higher energy state [12,40]. The Stokes shifts of compounds **4a–4d** in different solvents were calculated to know the structural reorganization occurring during electronic excitation. Stokes shift values in different solvents for the compounds follow the order **4a** < **4b** < **4c** < **4d**. Larger Stokes shift observed for **4d** indicates appreciable structural reorganization due to photo-excitation from ground state to excited state [34]. Furthermore, the relationships of Stokes shift against the solvent parameter $E_T(30)$ of the compounds **4a–4d** were investigated as shown in Fig. S6. The slopes of the correlation plots are in the order of **4c** (84.53) < **4b** (93.10) < **4d** (93.89) < **4a** (103.04), which indicates that more pronounced intramolecular charge transfer is occurred in compound **4a** [34].

3.3. Crystal structure and theoretical calculation

Suitable single crystals of compounds **4a** and **4b** for X-ray crystallography were obtained by the slow evaporation of a mixture of dichloromethane/hexane at room temperature. However, efforts to obtain the suitable single crystals of **4c** and **4d** were failed due to their limited solubility in common solvent. The detailed

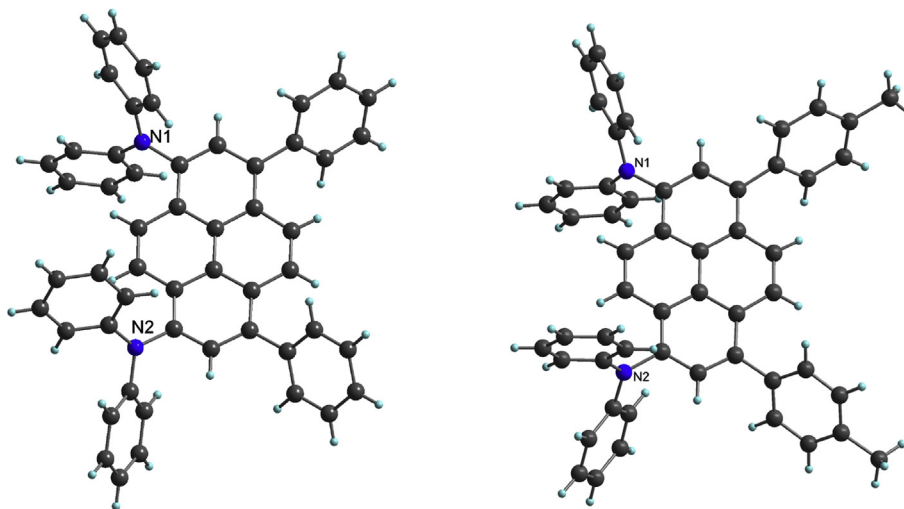


Fig. 3. X-ray structure diagram of the compounds **4a** (left) and **4b** (right).

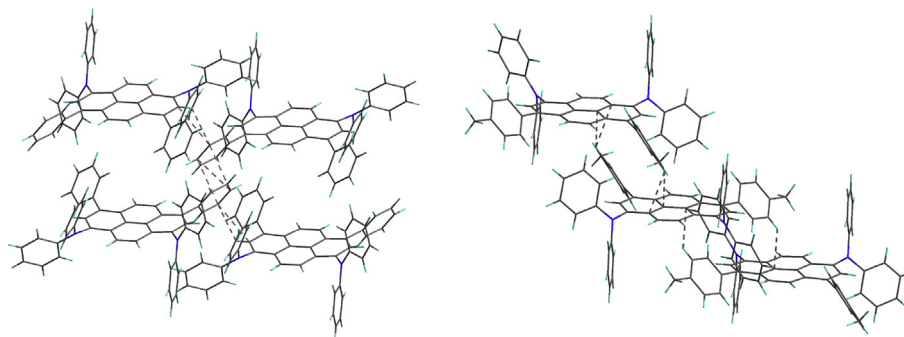


Fig. 4. Crystal packing diagram of **4a** (left) and **4b** (right).

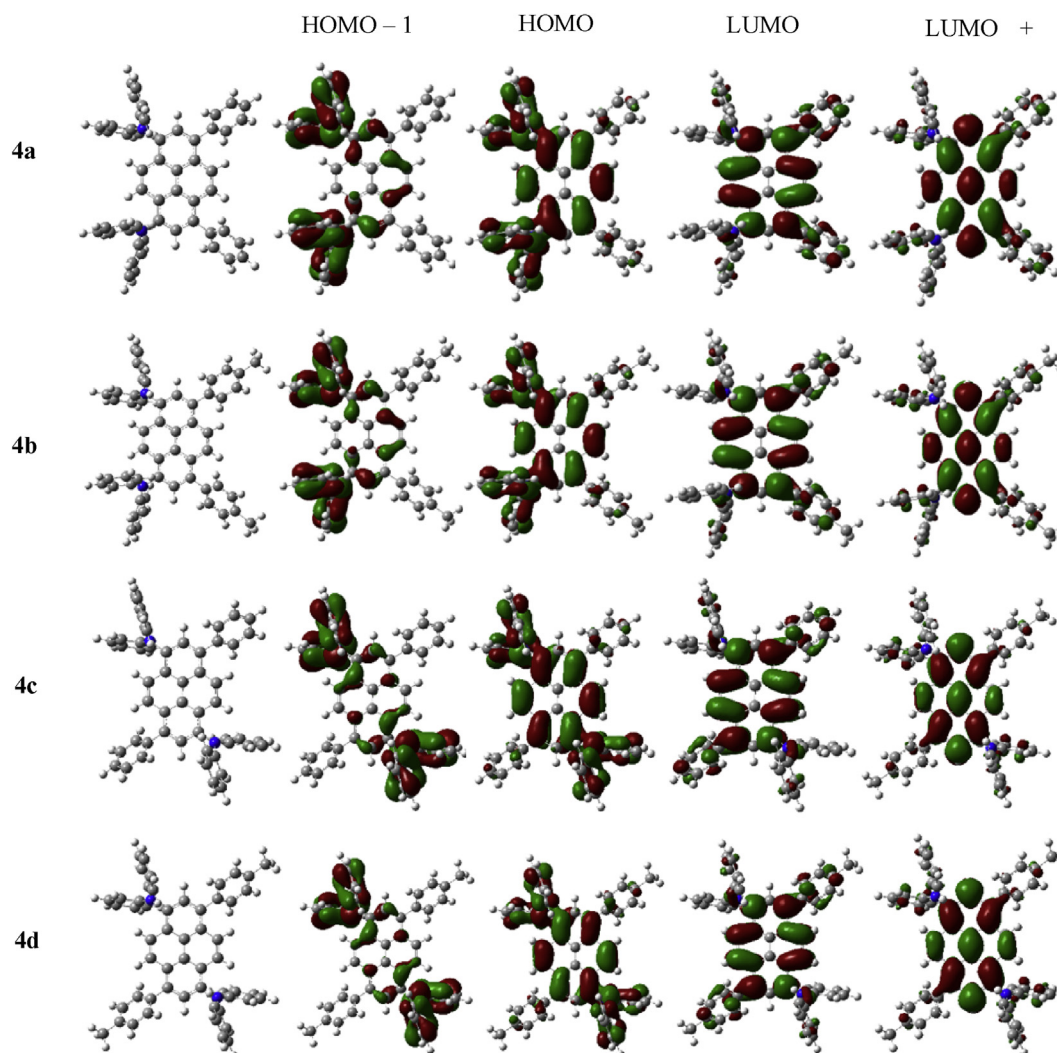


Fig. 5. Electronic distributions observed for the frontier orbitals for the compounds **4a–4d**.

information about the crystal data for compounds **4a** and **4b** is summarized in Table 3. Compounds **4a** and **4b** crystallize in the triclinic crystal system with space group $P\bar{1}$. The crystal structure diagrams of the two compounds are shown in Fig. 3.

X-ray diffraction analysis shows that the center pyrene cores of **4a** and **4b** are linked by two phenyl moieties at the 1, 8-positions and two diphenylamine attachments at the 3, 6-positions of the pyrene core. The bond lengths of C–N in the compounds are in a narrow range of 1.417(4)–1.428(4) Å for **4a** and 1.403(4)–1.448(4) Å for **4b**. The bond angles of C–N–C in the compounds **4a** and **4b** range from 116.82 (3) to 123.08 (3)°. In the two crystal structures,

the phenyl units attached on the 3, 6-positions of pyrene ring are completely not coplanar with the pyrene plane, which are evidenced by the dihedral angles are 57.76 (3)° and 54.14 (3)° for **4a** and **4b**, respectively. Of course, the pyrene cores are also twisted by diphenylamine units with the dihedral angle between pyrene and phenyl moieties in the range of 68.51(3)–87.42(3)° for **4a** and 78.67(3)–88.14(3)° for **4b**. The four atoms including the nitrogen atom and the three carbons bonded by nitrogen atom are almost coplanar with the maximal deviations of 0.022 (4) Å (N1) and 0.103 (4) Å (N2) for **4a**, 0.027 (4) Å (N1) and 0.067 (3) Å (N2) for **4b**.

The crystal packing diagrams of **4a** and **4b** are shown in Fig. 4. As

Table 2

Electrochemical and thermal properties of the compounds.

Com.	E_{ox} ^a mV	E_g^b/E_g cal. ^c (eV)	HOMO/LUMO ^d (eV)	HOMO/LUMO ^c (eV)	T_d/T_g (°C)
4a	0.385	2.64/2.99	–5.17/–2.53	–4.73/–1.74	358/146
4b	0.335	2.61/2.99	–5.17/–2.56	–4.68/–1.69	365/149
4c	0.285	2.58/2.87	–5.29/–2.71	–4.82/–1.95	399/ND
4d	0.265	2.57/2.86	–5.27/–2.70	–4.80/–1.94	408/ND

^a Measured in dry dichloromethane. All E_{ox} data are reported relative to ferrocene.

^b Calculated from the absorption edge, $E_g = 1240/\lambda_{\text{onset}}$.

^c Obtained from the quantum chemical calculation.

^d HOMO values were deduced from the relation: HOMO = $E_{\text{ox}} + 4.8$. LUMO values were calculated from the relation: band gap = HOMO – LUMO.

Table 3
Summary of the crystal data of **4a** and **4b**.

Parameter	4a	4b
Empirical formula	C ₅₃ H ₃₈ Cl ₂ N ₂	C ₅₄ H ₄₀ N ₂
<i>M_r</i> (g mol ⁻¹)	773.75	716.88
<i>T</i> /K	293	293
Wavelength (Å)	0.71073	0.71073
Crystal system	triclinic	triclinic
Space group	<i>P</i> -1	<i>P</i> -1
<i>a</i> /Å	11.347 (2)	10.885 (2)
<i>b</i> /Å	12.125 (2)	12.055 (2)
<i>c</i> /Å	14.684 (3)	15.992 (3)
α (°)	99.99 (3)	83.34 (3)
β (°)	97.84 (3)	87.20 (3)
γ (°)	98.09 (3)	70.47 (3)
<i>V</i> (Å ³)	1942.9 (7)	1964.3 (7)
<i>Z</i>	2	2
<i>D_{calc}</i> (g cm ⁻³)	1.323	1.212
<i>F</i> (000)	808.0	756.0
μ (mm ⁻¹)	0.209	0.070
Unique reflections	6861	9105
Observed reflections	5589	5969
Parameters	514	499
<i>R</i> (int)	0.0235	0.1036
<i>R</i> [<i>I</i> > 2 σ (<i>I</i>)]	0.0646	0.0713
<i>wR</i> ₂ (all data)	0.2377	0.1503
GOF on <i>F</i> ²	0.979	0.977

known to all, the efficient π -stacking in emitting materials could lead to extensive excimer formation in thin film with low quantum yields of fluorescence, which makes a big obstacle for the solid state applications in photoelectric devices. From Fig. 4, no intermolecular π - π interactions were observed in the two crystals due to the big sterically hindrance arising from the bulky diphenylamine groups

and phenyl moieties on the pyrene core. For **4a** and **4b**, two independent units are mainly linked by C–H $\cdots\pi$ interactions, forming two-dimensional layer-like supramolecular structures. It is note worthy that the intermolecular interactions of compound **4b** seem more weak than those of compound **4a** because the C–H $\cdots\pi$ intermolecular interactions of **4b** originate from methyl group hydrogen atoms other than aromatic ring hydrogen atoms of **4a**. Thus, the newly prepared compounds **4a** and **4b** with less intermolecular interactions suggests that they might be advantageous as promising emitters in solid state.

To deeply investigate the electronic structures, orbital energies, electron densities of the highest occupied molecular orbital (HOMO) and lowest occupied molecular orbital (LUMO) states of the compounds **4a–4d**, as well as to understand the absorption characteristics, density functional theory (DFT) calculations (B3LYP/6-31G (d, p) basis set) were performed on the three compounds with the Gaussian 09 W software package. Three-dimensional optimized geometries and electronic distributions in the frontier molecular orbitals of compounds **4a–4d** are shown in Fig. 5 and the HOMO–LUMO energy gaps (*E_g* cal.) were calculated and are presented in Table 2. The prominent wavelength vertical transitions and their assignments are summarized in Table 4. The calculated structures of compounds **4a–4d** reveal that all molecules adopt non-coplanar conformations. The electronic distributions of compounds **4a** and **4b** are symmetrical, which is different from **4c** and **4d** whose π -electrons are asymmetrical. The measured wavelength absorption peaks and energy gaps of these compounds are smaller than the theoretically forecast values but the changing tendencies are similar. The longest wavelength transitions are mainly due to the electronic excitation from the HOMO to LUMO, while the second absorptions largely result from the HOMO – 1 to LUMO

Table 4
Predicted (TDDFT B3LYP/6-31G (d,p)) vertical transitions and their assignments.

Com.	λ_{abs} (nm)	<i>f</i>	Assignment
4a	478.48	0.4359	HOMO \rightarrow LUMO (95.1%), HOMO – 2 \rightarrow LUMO (3.5%)
	433.41	0.0584	HOMO – 1 \rightarrow LUMO (96.6%)
	377.27	0.0664	HOMO \rightarrow LUMO + 1 (84.6%), HOMO – 3 \rightarrow LUMO (12.0%)
4b	476.44	0.4611	HOMO \rightarrow LUMO (95.0%), HOMO – 2 \rightarrow LUMO (3.5%)
	431.02	0.0606	HOMO – 1 \rightarrow LUMO (97.7%)
	376.92	0.0672	HOMO \rightarrow LUMO + 1 (84.9%), HOMO – 3 \rightarrow LUMO (11.5%)
4c	474.72	0.5056	HOMO \rightarrow LUMO (95.1%), HOMO – 2 \rightarrow LUMO (3.2%)
	431.52	2.8732	HOMO – 1 \rightarrow LUMO (99.0%)
	381.28	3.2518	HOMO \rightarrow LUMO + 1 (74.2%), HOMO – 2 \rightarrow LUMO (15.5%)
4d	473.37	0.5272	HOMO \rightarrow LUMO (95.1%), HOMO – 2 \rightarrow LUMO (3.2%)
	429.00	2.8901	HOMO – 1 \rightarrow LUMO (99.0%)
	382.24	3.2436	HOMO \rightarrow LUMO + 1 (70.3%), HOMO – 2 \rightarrow LUMO (19.8%)

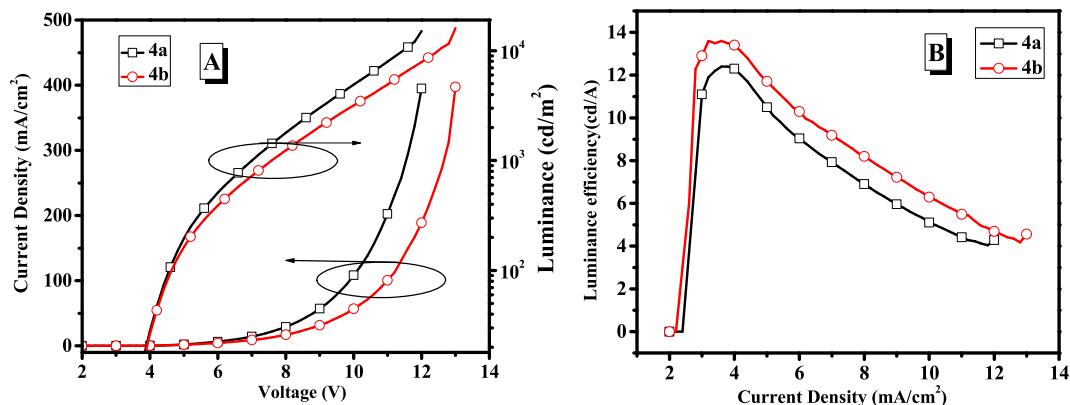


Fig. 6. The current density-voltage-luminance curves with varying thickness of the compounds **4a** and **4b** (A); Luminance efficiency of the compounds **4a** and **4b** (B).

Table 5EL performance: ITO/HAT-CN (5 nm)/NPB (30 nm)/CBP: 10 wt% **4a** or **4b** (25 nm)/Bphen (40 nm)/Cs₂CO₃ (2 nm)/Al (150 nm).

Devices	Emitters	V _{on} ^a (V)	EL _{max} ^b (nm)	L _{max} ^c at voltage (cd m ⁻² /V)	η _{max} ^d (cd/A)	EQE ^e (%)
I	4a	3.0	534	15100/12	12.4	5.34
II	4b	3.0	501	16100/13	13.6	5.63

^a Turn-on voltage (V) at a luminance of 1 cd m⁻².^b Emission maximum.^c Maximum luminance (cd m⁻²) at the applied voltage (V).^d Luminance efficiency (cd A⁻¹).^e External quantum efficiency (%).

electronic excitation. For compounds **4a–4d**, the HOMO orbitals are contributed by the diphenylamine and pyrene core, while the LUMO orbitals are mainly distributed over the electron-rich pyrenyl segments, which indicates that the longest absorption bands realized for **4a–4d** can be assigned to a charge transfer from pyrenylamine to pyrene. The π -electrons in the HOMO – 1 compounds **4a** and **4b** are mainly distributed on the diphenylamine unit and a little on the pyrene core, which indicates that the second transitions mainly stem from the charge transfer from the diphenylamine moieties to the pyrene core.

3.4. Electrochemical and thermal studies

The electrochemical properties of compounds **4a–4d** were studied by cyclic voltammetry (CV) measurements and the oxidation potentials of these compounds were calculated by calibrating with the internal ferrocene standard (Fig. S7). The relevant parameters are collected in Table 2. Compounds **4a–4d** display two quasi-reversible oxidation waves arising from the oxidation of the amine. The HOMO values of compounds **4a**, **4b**, **4c** and **4d** estimated from the onset potentials of oxidation peak are –5.17 eV, –5.17 eV, –5.29 eV and –5.27 eV, respectively. The LUMO values of these compounds calculated by HOMO and E_g are in the range from –2.53 to –2.71 eV. The HOMO values of compounds **4a** and **4b** with symmetrical structure are larger than **4c** and **4d** and more close to the barrier of ITO (–4.8 eV), which indicates that the hole-transporting abilities of **4a** and **4b** are better than those of compounds **4c** and **4d**.

The thermal properties of the compounds **4a–4d** were investigated by thermogravimetric analysis (TGA) and differential scanning calorimetry (DSC) under a nitrogen atmosphere, the relevant data are shown in Table 2 and Figs. S8 and S9. These compounds show high thermal stability and the decomposition temperatures (T_d) corresponding to 5% weight loss are 358, 365, 399 and 408 °C for compounds **4a**, **4b**, **4c** and **4d**, respectively. DSC thermograms of the compounds **4a** and **4b** display high glass transition temperature (T_g) values at 146 and 149 °C, respectively, and no crystallization and melting peaks being observed at higher temperatures, indicating an excellent amorphous glass state stability [41]. However, compound **4c** and **4d** do not show obvious T_g most likely due to their crystallinity and small heat capacity.

3.5. Electroluminescence

Two representative compounds **4a** and **4b** were employed as the doped emitting layers in OLEDs with the following configuration: ITO/HAT-CN (5 nm)/NPB (30 nm)/CBP: 10 wt% **4a** or **4b** (25 nm)/Bphen (40 nm)/Cs₂CO₃ (2 nm)/Al (150 nm). Here, 1,4,5,8,9,11-hexaazatriphenylene hexacarbonitrile (HAT-CN) acts as the hole injection layer, NPB as the hole-transporting layer (HTL), the **4a** or **4b**: 4,4'-bis(N-carbazolyl)-1,1'-biphenyl (CBP) guest–host systems were chosen as emitting-material layer, 1,10-Bathophenanthroline (Bphen) was conducted as electron-transporting layer (ETL). The

current density–voltage–luminance (J – V – L) characteristics and the current density–efficiency curves of the fabricated OLEDs are shown in Fig. 6. The essential performance electric parameters are demonstrated in Table 5. The turn-on voltages of the **4a**- (device **I**) and **4b**-based (device **II**) devices are very low with the values all of 3.0 V, which indicates that the performance of the devices is decent. The device **II** using **4b** as dopant shows the best device performance with a maximum brightness (L_{max}) of 16100 cd/m², a maximum luminance efficiency (η_{max}) of 13.6 cd/A, a maximum external quantum efficiency of 5.63%. The **4a**-based device exhibits a relatively lower device performance with an L_{max} of 15100 cd/m², a η_{max} of 12.4 cd/A, a maximum external quantum efficiency of 5.34%. The devices **I** and **II** emit strong green emission with λ_{EL} peaked at 534 nm and 501 nm, respectively. Furthermore, the electroluminescence (EL) spectra of the devices match with their corresponding PL spectra, indicating that the EL purely originate from the emitting layers.

4. Conclusions

In conclusion, a new series of short axially symmetrically and asymmetrically 1,3,6,8-tetrasubstituted pyrene-based derivatives with different substituents on the pyrene core have been elaborately designed and successfully synthesized. The crystal structures of **4a** and **4b** indicate that the molecule is twisted by the peripheral substituents and the intermolecular π – π interactions have been efficiently interrupted. Compounds **4a** and **4b** exhibit higher absolute fluorescence quantum yields than those of **4c** and **4d** in dichloromethane and as drop-coating films, which reveals the symmetrical structure can benefit to improve the PL properties of the compounds. Compounds **4a–4d** exhibit high thermal stability and the values of **4c** and **4d** are higher than **4a** and **4b**, indicating that the asymmetrical configuration can slightly increase thermal stability of the compounds. The compounds **4a** and **4b** can form morphologically stable amorphous thin films with T_g values of 146 °C and 149 °C, respectively. However, there are no obvious T_g observed in compounds **4c** and **4d**. Organic light-emitting diodes featuring compounds **4a** and **4b** as doped emission layer show promising device performance with low turn-on voltage (3.0 V), maximum brightness around 15100 cd/m² and 16100 cd/m², maximum luminance efficiency of 12.4 cd/A and 13.6 cd/A and maximum external quantum efficiency of 5.34% and 5.63%, respectively.

Acknowledgements

This work was supported by the Fundamental Research Funds for the Central Universities (2015XKZD08) and the Priority Academic Program Development of Jiangsu Higher Education Institutions.

Appendix A. Supplementary data

Supplementary data related to this article can be found at <http://dx.doi.org/10.1016/j.molstruc.2016.07.105>.

References

- [1] K.C. Stylianou, R.H. Samantha, Y. Chong, J. Bacsá, J.T.A. Jones, Y.Z. Khimyak, D. Bradshaw, M.J. Rosseinsky, A guest-responsive fluorescent 3D microporous metal-organic framework derived from a long-lifetime pyrene core, *J. Am. Chem. Soc.* 132 (2010) 4119–4130.
- [2] J.C. Wu, Y. Zou, C.Y. Li, W. Sicking, I. Piantanida, T. Yi, C. Schmuck, A molecular peptide beacon for the ratiometric sensing of nucleic acids, *J. Am. Chem. Soc.* 134 (2012) 1958–1961.
- [3] K.R.J. Thomas, N. Kapoor, M.N.K. Prasad Bolisetty, J.H. Jou, Y.L. Chen, Y.C. Jou, Pyrene-fluorene hybrids containing acetylene linkage as color-tunable emitting materials for organic light-emitting diodes, *J. Org. Chem.* 77 (2012) 3921–3932.
- [4] B. Kim, Y. Park, J. Lee, D. Yokoyama, J.H. Lee, J. Kido, J. Park, Synthesis and electroluminescence properties of highly efficient blue fluorescence emitters using dual core chromophores, *J. Mater. Chem. C* 1 (2013) 432–440.
- [5] I.V. Astakhova, V.A. Korshun, J. Wengel, Highly fluorescent conjugated pyrenes in nucleic acid probes: (phenylethynyl)pyrenecarbonyl-functionalized locked nucleic acids, *Chem. Eur. J.* 14 (2008) 11010–11026.
- [6] B.R. Kaafarani, L.A. Lucas, B. Wex, G.E. Jabbour, Synthesis of novel pyrene discotics for potential electronic applications, *Tetrahedron Lett.* 48 (2007) 5995–5998.
- [7] H. Lee, B. Kim, S. Kim, J. Kim, J. Lee, H. Shin, J.H. Lee, J. Park, Synthesis and electroluminescence properties of highly efficient dual core chromophores with side groups for blue emission, *J. Mater. Chem. C* 2 (2014) 4737–4747.
- [8] R. Zhang, Y. Zhao, G.L. Li, D.S. Yang, Z.H. Ni, A new series of pyrenyl-based triarylamines: syntheses, structures, optical properties, electrochemistry and electroluminescence, *RSC Adv.* 6 (2016) 9037–9048.
- [9] Z.M. Zhang, Y. Zhao, R. Zhang, L.F. Zhang, W.Q. Cheng, Z.H. Ni, Design and synthesis of a new series of tetra(polycyclic aryl)ethenes: achieving aggregation-induced emission and efficient solid-state photoluminescence, *Dyes Pigments* 118 (2015) 95–101.
- [10] T.M. Figueira-Duarte, K. Müllen, Pyrene-based materials for organic electronics, *Chem. Rev.* 111 (2011) 7260–7314.
- [11] K.R.J. Thomas, J.T. Lin, Y.T. Tao, C.W. Ko, Novel green light-emitting carbazole derivatives: potential electroluminescent materials, *Adv. Mater.* 12 (2000) 1949–1951.
- [12] R. Zhang, L.H. Xu, H. Chen, Z.H. Qin, Y. Zhao, Z.H. Ni, Convenient synthesis of 1-thiohydroxypyrene by Newman-Kwart rearrangement, *Chem. Res. Chin. Univ.* 31 (2015) 224–227.
- [13] A.G. Crawford, Z.Q. Liu, I.A.I. Mkhallid, M.H. Thibault, N. Schwarz, G. Alcaraz, A. Steffen, J.C. Collings, A.S. Batsanov, J.A. Howard, T.B. Marder, Synthesis of 2- and 2,7-functionalized pyrene derivatives: an application of selective C-H borylation, *Chem. Eur. J.* 18 (2012) 5022–5035.
- [14] Y.L. Liu, T. Shan, L. Yao, Q. Bai, Y.C. Guo, J.Y. Li, X. Han, W.J. Li, Z.M. Wang, B. Yang, P. Lu, Y.G. Ma, Isomers of pyrene-imidazole compounds: synthesis and configuration effect on optical properties, *Org. Lett.* 17 (2015) 6138–6141.
- [15] X. Feng, J.Y. Hu, X.F. Wei, C. Redshaw, T. Yamato, Influence of substituent position on thermal properties, photoluminescence and morphology of pyrene-fluorene derivatives, *J. Mol. Struct.* 1086 (2015) 216–222.
- [16] Z.M. Zhang, F.F. Han, R. Zhang, N. Li, Z.H. Ni, Design, syntheses and aggregation-induced emission properties of two new enlarged tetraarylethene-based luminogens, *Tetrahedron Lett.* 57 (2016) 1917–1920.
- [17] Y. Niko, S. Kawachi, S. Otsu, K. Tokumaru, G.i. Konishi, Fluorescence enhancement of pyrene chromophores induced by alkyl groups through σ - π conjugation: systematic synthesis of primary, secondary, and tertiary alkylated pyrenes at the 1, 3, 6, and 8 positions and their photophysical properties, *J. Org. Chem.* 78 (2013) 3196–3207.
- [18] T. Keawin, N. Prachumrak, S. Namuangruk, S. Pansay, N. Kungwan, S. Maensiri, S. Jungstittiwong, T. Sudyoadsuk, V. Promarak, Efficient bifunctional materials based on pyrene- and triphenylamine-functionalized dendrimers for electroluminescent devices, *RSC Adv.* 5 (2015) 73481–73489.
- [19] F. Liu, C. Tang, Q.Q. Chen, S.Z. Li, H.B. Wu, L.H. Xie, B. Peng, W. Wei, Y. Cao, W. Huang, Pyrene functionalized diarylfluorenes as efficient solution processable light emitting molecular glass, *Org. Electron* 10 (2009) 256–265.
- [20] Y.J. Pu, M. Higashidate, K.i. Nakayama, J. Kido, Solution-processable organic fluorescent dyes for multicolor emission in organic light emitting diodes, *J. Mater. Chem.* 18 (2008) 4183–4188.
- [21] T.M. Figueira-Duarte, S.C. Simon, M. Wagner, S.I. Druzhinin, K.A. Zachariasse, K. Müllen, Polypyrene dendrimers, *Angew. Chem. Int. Ed.* 47 (2008) 10175–10178.
- [22] J.Y. Hu, X. Feng, H. Tomiyasu, N. Seto, U. Rayhan, M.R.J. Elsegood, C. Redshaw, T. Yamato, Synthesis and fluorescence emission properties of 1,3,6,8-tetraarylpirenes, *J. Mol. Struct.* 1047 (2013) 194–203.
- [23] X. Feng, H. Tomiyasu, J.Y. Hu, X.F. Wei, C. Redshaw, M.R.J. Elsegood, L. Horsburgh, S.J. Teat, T. Yamato, Regioselective substitution at the 1,3- and 6,8-Positions of pyrene for the construction of small dipolar molecules, *J. Org. Chem.* 80 (2015) 10973–10978.
- [24] Z.J. Zhao, S.M. Chen, J.W.Y. Lam, P. Lu, Y.C. Zhong, K.S. Wong, H.S. Kwok, B.Z. Tang, Creation of highly efficient solid emitter by decorating pyrene core with AIE-active tetraphenylethene peripheries, *Chem. Commun.* 46 (2010) 2221–2223.
- [25] M. Sase, S. Yamaguchi, Y. Sagara, I. Yoshikawa, T. Mutai, K. Araki, Piezochromic luminescence of amide and ester derivatives of tetraphenylpyrene—role of amide hydrogen bonds in sensitive piezochromic response, *J. Mater. Chem.* 21 (2011) 8347–8354.
- [26] H. Maeda, T. Maeda, K. Mizuno, K. Fujimoto, H. Shimizu, M. Inouye, Alkynylpyrenes as improved pyrene-based biomolecular probes with the advantages of high fluorescence quantum yields and long absorption/emission wavelengths, *Chem. Eur. J.* 12 (2006) 824–831.
- [27] A. Hayer, V. Halleux, A. Köhler, A. El-Garouhy, E.W. Meijer, J. Barberá, J. Tant, J. Levin, M. Lehmann, J. Gierschner, Jérôme Cornil, Y.H. Geerts, Highly fluorescent crystalline and liquid crystalline columnar phases of pyrene-based structures, *J. Phys. Chem. B* 110 (2006) 7653–7659.
- [28] K. Fujimoto, H. Shimizu, M. Furusyo, S. Akiyama, M. Ishida, U. Furukawa, T. Yokoo, M. Inouye, Photophysical properties of 1,3,6,8-tetrakis(arylethynyl)pyrenes with donor or acceptor substituents: their fluorescence solvatochromism and lightfastness, *Tetrahedron* 65 (2009) 9357–9361.
- [29] R. Zhang, Y. Zhao, T.F. Zhang, L. Xu, Z.H. Ni, A series of short axially symmetric 1,3,6,8-tetrasubstituted pyrene-based green and blue emitters with 4-*tert*-butylphenyl and arylamine attachments, *Dyes Pigments* 130 (2016) 106–115.
- [30] V.L. Malinovskii, R. Häner, Synthesis of polysubstituted pyrenes with tuned spectroscopic properties for two-point attachment, *Eur. J. Org. Chem.* 16 (2006) 3550–3553.
- [31] G.M. Sheldrick, A short history of SHELX, *Acta Crystallogr. Sect. A Found. Crystallogr.* A64 (2008) 112–122.
- [32] M.J. Frisch, G.W. Trucks, H.B. Schlegel, G.E. Scuseria, M.A. Robb, J.R. Cheeseman, Gaussian 09, Revision A.02, Gaussian, Inc., Wallingford, CT, 2009.
- [33] J. Grimshaw, J. Trocha-Grimshaw, Characterisation of 1,6- and 1,8-dibromopyrenes, *J. Chem. Soc. Perkin Trans. 1* (1972) 1622–1623.
- [34] D. Karthik, K.R.J. Thomas, J.H. Jou, S. Kumar, Y.L. Chen, Y.C. Jou, Deep-blue emitting pyrene-benzimidazole conjugates for solution processed organic light emitting diodes, *RSC Adv.* 5 (2015) 8727–8738.
- [35] K.R. Justin Thomas, M. Velusamy, J.T. Lin, C.H. Chuen, Y.T. Tao, Hexaphenylphenylene dendronised pyrenylamines for efficient organic light-emitting diodes, *J. Mater. Chem.* 15 (2005) 4453–4459.
- [36] H.Y. Oha, C. Lee, S. Lee, Efficient blue organic light-emitting diodes using newly-developed pyrene-based electron transport materials, *Org. Electron* 10 (2009) 163–169.
- [37] H.C. Liu, Q. Bai, L. Yao, H.Y. Zhang, H. Xu, S.T. Zhang, W.J. Li, Y. Gao, J.Y. Li, P. Lu, H.Y. Wang, B. Yang, Y.G. Ma, Highly efficient near ultraviolet organic light-emitting diode based on a *meta*-linked donor-acceptor molecule, *Chem. Sci.* 6 (2015) 3797–3804.
- [38] T. Oyamada, S. Akiyama, M. Yahiro, M. Saigou, M. Shiro, H. Sasabe, C. Adachi, Unusual photoluminescence characteristics of tetraphenylpyrene (TPPy) in various aggregated morphologies, *Chem. Phys. Lett.* 421 (2006) 295–299.
- [39] F.M. Winnik, Photophysics of preassociated pyrenes in aqueous polymer solutions and in other organized media, *Chem. Rev.* 93 (1993) 587–614.
- [40] N. Kapoor, K.R.J. Thomas, Fluoranthene-based triarylamines as hole-transporting and emitting materials for efficient electroluminescent devices, *New J. Chem.* 34 (2010) 2739–2748.
- [41] A. Thangthong, N. Prachumrak, R. Tarsang, T. Keawin, S. Jungstittiwong, T. Sudyoadsuk, V. Promarak, Blue light-emitting and hole-transporting materials based on 9,9-bis(4-diphenylaminophenyl)fluorenes for efficient electroluminescent devices, *J. Mater. Chem.* 22 (2012) 6869–6877.